

Is Young's Modulus a Critical Coating Property Determining Fouling-Release Performance of Marine Coatings?

Johann C. Schaal, Andreas Brinkmann,* and Andreas Hartwig

Marine organisms colonize all water-contacting surfaces. The accumulation of these organisms, known as biofouling, on ship hulls can increase fuel consumption by up to 45%, causing higher emissions. Remedy is offered by nonbiocidal fouling-release (FR) coatings, which weaken the adhesion between organisms and surfaces, enabling removal by hydrodynamic forces or gravity. This study investigates the FR performance of biocide-free polyurethane, polyurea, and silicone-based systems in relation to their Young's modulus. The rationale is to better understand the influence of Young's modulus across different polymer classes. Within these classes, Young's modulus varies in a narrow range (0.2–2.2 MPa) to study its effect on FR behavior. In polyurethane and polyurea systems, modulus adjustments are made by altering resin-to-hardener ratios, affecting crosslink density. Coatings underwent static immersion in the North Sea, and FR performance is monitored monthly. After 15 weeks, samples are cleaned with a high-pressure water jet. Compared to a hard reference system, all soft coatings exhibit FR performance identical to Intersleek 1100 SR after full immersion period and cleaning, highlighting the importance of mechanical softness for effective fouling release.

application of such materials is the reduction of biofouling on water-contacting surfaces, such as ship hulls or offshore structures. The challenge is to design the surface's chemical, physical, and mechanical properties in such a way that bioadhesion is reduced, ideally eliminated, to mitigate negative economic and ecological consequences.^[1–3] Specifically, in shipping, this means a potential reduction in fuel consumption by up to 45% and a decrease in the spread of invasive marine organisms.^[2]

Antifouling coatings can be fundamentally divided into biocide-based and biocide-free coatings, which follow two different approaches. Biocide-based antifouling coatings prevent the settlement of organisms, whereas fouling-release coatings (FRCs) sufficiently weaken the adhesion between organisms and the surface to allow the removal of biomass through hydrodynamic stress,^[4] or by its own weight.

Due to the harmful effects of biocide-emitting antifouling coatings, especially those based on organotin compounds, cybutryne, copper thiocyanate, and dicopper oxide, their use is regulated at both national and international levels.^[1,5–7] This has led to a growing interest in the development of more ecological coatings as an alternative to traditional technologies. Alternatives include antifouling coatings based on contact biocides, such as quaternary ammonium agents.^[8–10] In these systems, the agents are covalently incorporated into the polymer matrix and are not released into the environment and do not have a negative impact on the ecosystem. Nonbiocidal FRCs are based, for example, on amphiphilic structures that feature both hydrophilic and hydrophobic domains.^[11–15] A specific case involves the use of zwitterions,^[16–21] which have a high proportion of ionic groups with a neutral net charge and exhibit strong hydrophilicity. These zwitterions reduce the adsorption of organisms in aqueous environments.^[21] Other design possibilities include the use of hard–soft segments or surface structuring as driving forces for fouling release.^[22–24]

It is well known from nature and technology that different requirements must be met for adhesion bond on a surface, depending on whether the substrate has a hard or an elastically soft surface. Only when these requirements are fulfilled can sufficient adhesion be ensured. Not every fouling organism is able to develop a universal strategy to attach and settle on surfaces with different mechanical properties. That is why, fundamental


1. Introduction

Uncontrolled interactions between biological species and nonbiological surfaces justify the ongoing development of materials that make interactions at interfaces more controllable. One

J. C. Schaal, A. Brinkmann, A. Hartwig
Fraunhofer Institute for Manufacturing Technology and Advanced Materials (IFAM)
Wiener Str. 12, 28359 Bremen, Germany
E-mail: andreas.brinkmann@ifam.fraunhofer.de

J. C. Schaal, A. Hartwig
Department Biology/Chemistry
University of Bremen
Leobener Str. 3, 28359 Bremen, Germany

A. Hartwig
MAPEX Center for Materials and Processes
University of Bremen
Bibliothekstraße 1, 28359 Bremen, Germany

 The ORCID identification number(s) for the author(s) of this article can be found under <https://doi.org/10.1002/adem.202501661>.

© 2025 The Author(s). Advanced Engineering Materials published by Wiley-VCH GmbH. This is an open access article under the terms of the Creative Commons Attribution License, which permits use, distribution and reproduction in any medium, provided the original work is properly cited.

DOI: 10.1002/adem.202501661

studies suggest that Young's modulus is a critical factor in significantly shaping the performance of FRCs.

Based on a fracture mechanical model, Brady and Chaudhury et al. show that the critical force P_c , required to separate two surfaces after adhesion, is correlated to the Young's modulus.^[25–27] In the scope of biomedical studies,^[2,28–30] Baier illustrates the fundamental relationship between relative adhesion and the surface energy of a polymer system plotted in the Baier curve. Interestingly, polymer systems showing a minimum in relative adhesion, also feature low Young's moduli. Zhang et al. demonstrate through benthic diatom adhesion tests that the reduction of the Young's modulus of polyurethane systems leads to an improvement in fouling-release properties.^[23] Further, Xi et al. worked with a nonsilicone coating based on degradable hyperbranched poly(ϵ -caprolactone) cross-linked with an amphiphilic triblock copolymer PEG–PPG–PEG. It was shown that the fouling-release properties improve with the increase in the PEG–PPG–PEG content and the corresponding decrease in the Young's modulus.^[31] Chaudhury et al. also demonstrated that soft silicone (PDMS) systems with low Young's modulus exhibit a higher release of soft foulers compared to PDMS systems with higher Young's modulus.^[32] Also, in the context of cell therapy, the relationship between the Young's modulus and fouling plays a role. Jalali et al. show that the endothelial cell adherence can be controlled by the substrates' Young's modulus.^[33]

A direct comparison between a high-performance FRC and different polymer classes with similar—in ideal case identical—low Young's moduli and the consideration of the resulting effect on their fouling-release efficiencies is still lacking.

Hence, in the context of this work, the first objective was to investigate whether projecting the low Young's modulus of the high-performing FRC Intersleek 1100 SR onto polyurea and polyurethane systems which are usually characterized by much higher Young's moduli leads to a corresponding improvement of fouling-release properties. For this reason, the Young's modulus of the mentioned polymer systems was adjusted to the Intersleek's Young's modulus, by changing the hardener–resin ratios. The second objective of this work was to investigate the influence of the variation of the Young's modulus within the polymer classes on their fouling-release efficiencies. The performance tests were carried out by static immersion at the island of Helgoland in the North Sea for 15 weeks. At the end of the immersion period, cleanability was assessed by treating the samples with a high-pressure water jet as an indication of the coatings' fouling-release behavior.

2. Experimental Section

2.1. Raw Materials

For both the polyurethane and the polyurea systems, the aliphatic polyisocyanate (HDI trimeric, Desmodur ultra N 3600, Covestro Deutschland AG) was used as curing agent. Applied polyester-polyol (Desmophen 1700) and hydroxyl-bearing polycarbonate polyester (Desmophen C1200) were provided by Covestro Deutschland AG. Carbinol-terminated siloxane HANSA SFA 92135 (3.9% OH– content), HANSA SFA 92057 (1.6% OH– content), and HANSA SFA 92024 (0.6% OH– content) were

provided by CHT Germany GmbH. For polyurea systems, amino functional binder (Desmophen NH1720) was used and provided by Covestro Deutschland AG. For polydimethylsiloxane systems, the reactants hydride-terminated poly(dimethylsiloxane) (AB109366), methylhydrosiloxane–dimethylsiloxane copolymer (AB109380), and vinyldimethylsiloxy-terminated polydimethylsiloxane (AB109356) were purchased from abcr, Germany. The catalyst platinum-(0)-1,3-divinyl-1,3,3,3-tetramethylidisiloxane was purchased from Merck, Germany. Akzo Nobel International Paints high-performing, fluoropolymer FRC Intersleek 1100 SR with its tie coat Intersleek 731 was used as a reference system. The Stelpant-PU-Combination 300 (brown) was used as negative reference (NR) and was purchased from Steelpaint GmbH. The Aerodur Barrier Primer 37045 was purchased from Akzo Nobel and used as a primer for all coatings.

2.2. Preparation of Polymer Coatings

The positive reference (PR) Intersleek 1100 SR was prepared according to the manufacturer's specified mixing ratios (75 parts A:15 parts B:10 parts C, by weight). The NR Stelpant-PU-Combination 300 (brown) was also prepared according to the manufacturer's specifications. Furthermore, both PR and NR were cured for 120 h at 60 °C. The coatings were denoted as follows: The coatings were divided in polymer types (polyurethane, polyurea, PDMS, PR, and NR). Polymer types were divided in polymer classes, depending on its binder type and denominated from A to E. Each polymer class was further divided in polymer systems depending on the binder-to-hardener ratio used and denominated by numbers beginning from 1. Denominations and specifications are given in **Table 1**. Compositions of PDMS-based coatings are given in **Table 2**. The formulations are described as follows. Polymer systems of classes A, B, C, and D were prepared via polyaddition reaction of polyisocyanates and polyols or polyamines. For systems of classes A, B, and C, the variation in Young's modulus was intended to be tailored by the variation of the NCO amount. For polymer systems of class D, the variation in Young's modulus was intended to be tailored by varying the HANSA SFA types with different hydroxy amounts and for systems of class E with the amount of hydride terminated poly(dimethylsiloxane) (component 1, **Table 2**) (bifunctional, linear linking) and methylhydrosiloxane-dimethylsiloxane copolymer (polyfunctional, crosslinking) (component 2, **Table 2**).

The resin–hardener ratio for polyurethane and polyurea systems was determined by using data from **Table 1** in Equation (1).

$$m_{\text{Hardener}} [\text{g}] = \left(\frac{M_{\text{eq,Hardener}} [\text{g mol}^{-1}] \cdot n_{\text{eq,Hardener}} [\text{mol}]}{M_{\text{eq,Resin}} [\text{g mol}^{-1}] \cdot n_{\text{eq,Resin}} [\text{mol}]} \right) m_{\text{Resin}} [\text{g}] \quad (1)$$

For systems of classes A, B, and C, the NCO-based hardener was added to the binder, and both were mixed with the Speedmixer (Hauschild, DAC 700.1 FVZ, speed program 10 s at 800 rpm, 10 s 1000 rpm, 1 min at 1500 rpm, 3 min at 1800 rpm, and 3 min at 2000 rpm) or t_3 according to **Table 3**.

For class D, the siloxane binders (HANSA SFA 92024, 92075, and 92135) and the hardener Desmodur Ultra N 3600 were not miscible with each other. Hence, crosslinking of the binder and

Table 1. Composition and denomination of the polyurethane and polyurea polymer types with the OH-content, equivalent weights (M_{eq}) according to the manufacturer's datasheet, and the equivalent amount of substance n_{eq} .

Polymer type	Polymer class	Polymer system	Resin	Reactive group, resin	$M_{eq,Resin}$ [g mol ⁻¹]	Hardener	Reactive group, hardener	$M_{eq,Hardener}$ [g mol ⁻¹]	$n_{eq,Resin}/n_{eq,Hardener}$ [mol/mol]	$n_{eq,Resin}/n_{eq,Hardener}$ [mol%/mol%]	$m_{Resin}/m_{Hardener}$ [w%/w%]		
Polyurethane	A	A3	Desmophen 1700	Hydroxy	1310	Desmodur Ultra N 3600	Isocyanate	183	1.00/1.00	50/50	87.73/12.27		
		A2							1.00/0.81	55.25/44.75	89.83/10.17		
		A1							1.00/0.62	61.73/38.27	92.02/7.98		
	B	B3	Desmophen C1200	Hydroxy	1000					1.00/0.75	57.14/42.86	86.69/13.31	
		B2								1.00/0.70	58.82/41.18	88.64/11.36	
		B1								1.00/0.65	60.60/39.40	89.36/10.64	
	D	D1	HANSA SFA 92135 (3.9% OH)	Hydroxy	432					1.00/1.00	50/50	70.72/29.75	
		D2								HANSA SFA 92075 (1.6% OH)	1.00/1.00	50/50	85.05/14.95
		D3								HANSA SFA 92024 (0.6% OH)	1.00/1.00	50/50	94.1/5.90
Polyurea	C	C2	Desmophen NH1720	Amine	295				1.00/0.80	55.56/44.44	66.82/33.18		
		C1							1.00/0.65	60.61/39.39	71.27/28.73		

Table 2. PDMS-based coating compositions.

Polymer type	Polymer class	Component no.	Compound	Polymer system		
				E1 [w%]	E2 [w%]	E3 [w%]
PDMS	E	1	Poly(dimethylsiloxane), hydride terminated	9.07	14.07	19.07
		2	Methylhydrosiloxane-dimethylsiloxane copolymer	28.61	26.95	25.28
		3	Polydimethylsiloxane, vinyl dimethylsiloxo terminated	43.20	41.54	39.87
		4 ^{a)}	Platinum-(0)-1,3-divinyl-1,3,3,3-tetramethylsiloxane in polydimethylsiloxane, vinyl dimethylsiloxo terminated	19.09	17.42	15.76

^{a)}Composition of component 4 is 0.2 mg Karstedt catalyst dissolved in 1 g vinyl dimethylsiloxo-terminated polydimethylsiloxane.

Table 3. Mixing times, curing times, and curing temperatures for prepared coating compositions.

Polymer class	Polymer system	Dispermat		Speedmixer		Curing	
		t_1 [min]	t_2 [min]	t_3 [min:sec]	t_4 [min:sec]	T_{curing} [°C]	t_{curing} [h]
A	A1, A2, A3	n/a	n/a	07:20	n/a	60	120
B	B1, B2, B3	n/a	n/a	07:20	n/a	60	120
D	D1	5	30	01:20	n/a	60	220
	D2	5	60 ± 10	01:20	n/a	60	220
	D3	5	31 ± 4	01:20	n/a	60	220
C	C1, C2	n/a	n/a	07:20	n/a	60	120
E	E1, E2, E3	n/a	n/a	2	00:50	RT	220

hardener was achieved through emulsification and the addition of a catalyst. At the end, the material was degassed and doctor-bladed or cast onto the substrates. In detail, for system D, the hardener Desmodur Ultra N 3600 was added to the HANSA SFA binders, and both were mixed with a Dispermat (Getzmann, Typ 6Fu2-548, disc diameter 2.7 cm, paint cup

150 mL, and speed 8000 rpm) for t_1 . Then, the catalyst TIBKAT 716 ($m\% = 0.02$) was added, and the mixture was mixed with the Dispermat for t_2 and degassed with the Speedmixer for t_3 , according to Table 3.

Polymer systems of class E were prepared by hydrosilylation. Components 1, 2, and 3 (Figure 1 and Table 2) were mixed with a

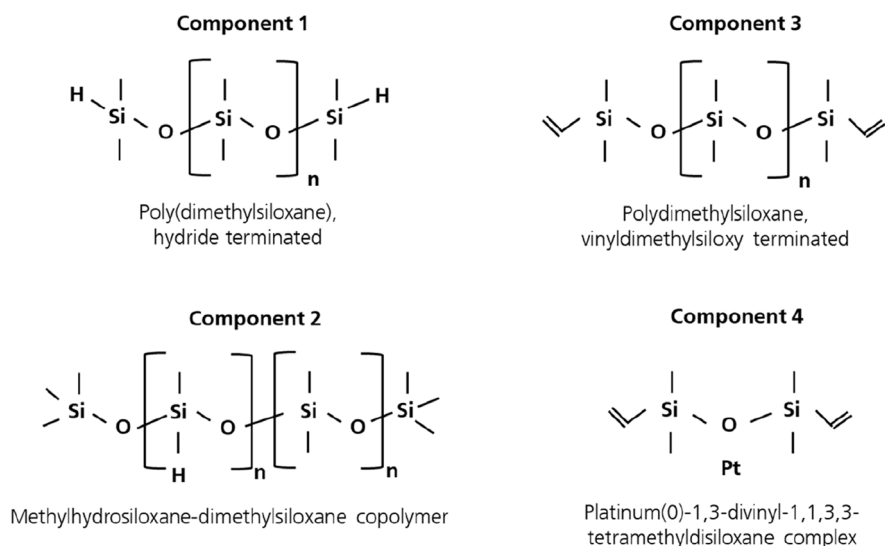


Figure 1. Structures of used components for hydrosilylation reaction to form PDMS-based polymer systems of class E.

Speedmixer for t_3 . Subsequently, component 4 was added and the system was mixed for t_4 according to Table 3.

2.3. Pendulum Hardness, Surface Free Energy, and Shore Hardness

The polymer systems according to Section 2.2 were poured into glass molds with dimensions of $65 \times 50 \times 1.4$ mm and were cured at the curing temperature T_{curing} as specified in Table 3. The curing process was monitored daily using the König pendulum hardness tester (BYK Gardner GmbH, Cat. No.: 5854), according to the procedures outlined in DIN 1522:1999. Measurements were carried out at 20°C .

The surface free energies (SFEs) of the coatings were measured by dynamic contact angle, according to DIN EN 19403:2020, using a Krüss Drop Shape Analyzer (DSA100, V2-05, ethylene glycol anhydrous 99.8% from Sigma-Aldrich, Chromasolv Plus for HPLC from Honeywell). Additionally, Shore 00 hardness (HP – Shore 00, Bareiss GmbH) was measured.

2.4. Tensile Measurement

The polymer systems according to Section 2.2 were poured into a polypropylene mold of $90 \times 60 \times 1.4$ mm. Then, the samples were cured at temperature T_{curing} (Table 3). Afterward, the films were peeled off and punched out to three standardized specimens (Type S2). Finally, tensile tests were conducted to

determine the Young's modulus according to DIN 53504 and DIN 527-1. The test parameters are listed in Table 4.

2.5. Preparation of Samples for Immersion in the North Sea

Self-machined PVC substrates (Figure 2 and 3, left) with the dimensions of 10.5×10.5 cm, a central recess of $10 \times 10 \times 0.14$ cm, and self-machined PVC holder (Figure 3, right) were ground with a sandpaper (grain 350), degreased, primed with Aerodur 37045, and dried at room temperature (RT) for 24 h. Then, the frame systems and the edge of the PVC substrates were coated with Intersleek 731 and dried at ambient conditions for 24 h. Subsequently, Intersleek 1100 SR was applied on the border edges and dried at ambient conditions for 24 h. Finally, the polymer systems were cast into the recesses of the PVC substrates and dried at temperature T_{curing} according to Table 3. The thickness of all systems was 0.14 cm. Six replicates were made for each polymer system. Then, the samples were mounted into frames (Figure 3) and immersed at a floating raft in the south harbor of the island of Helgoland, German Bight, North Sea (Figure 4, left), ≈ 20 cm under the water surface (Figure 4, right). In order to identify the effect of the coating systems, it was ensured that fouling development proceeded through different phases. These included the initial fouling, characterized by biofilm formation, followed by the development of microfouling, and subsequently the formation of macrofouling. All three phases occurred within an immersion period over one season. The immersion period of 15 weeks started in July 2023 and ended in October 2023.

Table 4. Tensile testing parameters.

Tensile testing machine	Load cell	Extensometer	Preforce	Speed preforce	Clamping length	Young's modulus determination-strain range	Extensometer reference length	Test speed	Specimen holder
Zwick (Z2.5)	1 kN	MakroXtens II	0.1 N	15 mm min^{-1}	48 mm	0.05%–0.25%	20 mm	200 mm min^{-1}	2.5 kN

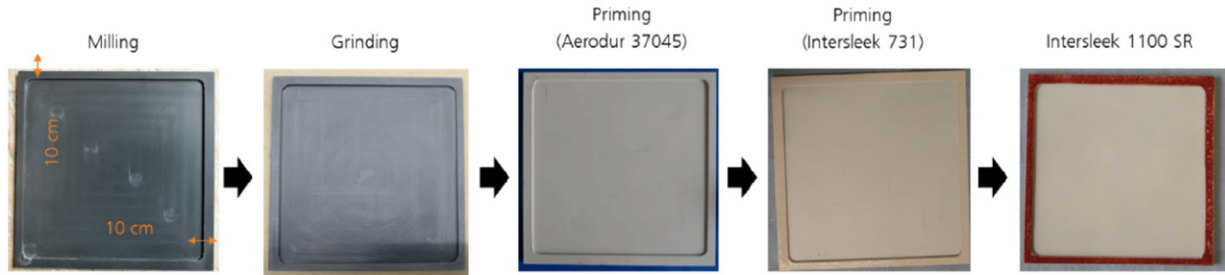


Figure 2. Preparation process of PVC substrates starting with milling, followed by grinding and priming. The final coating (Intersleek 1100 SR) is applied on the frame (red frame, left) to suppress fouling on it.

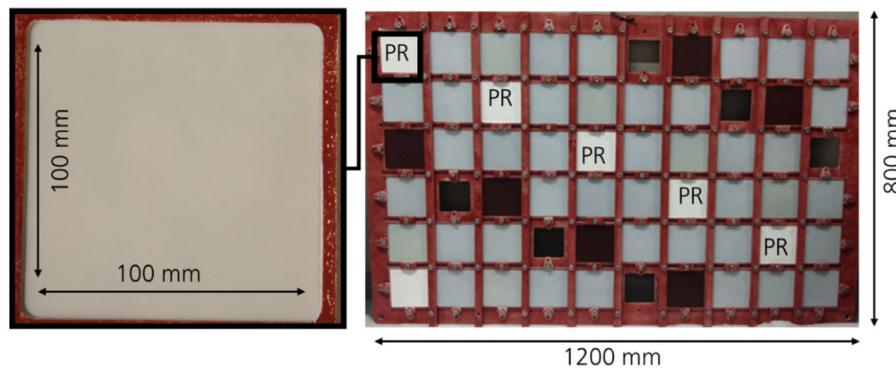


Figure 3. Single PVC substrate including dimensions for selected polymer systems according to Table 1 (left). Fixed PVC substrate in PVC holder. White fields (PR) show the arrangement scheme of the six replicates as an example (right).

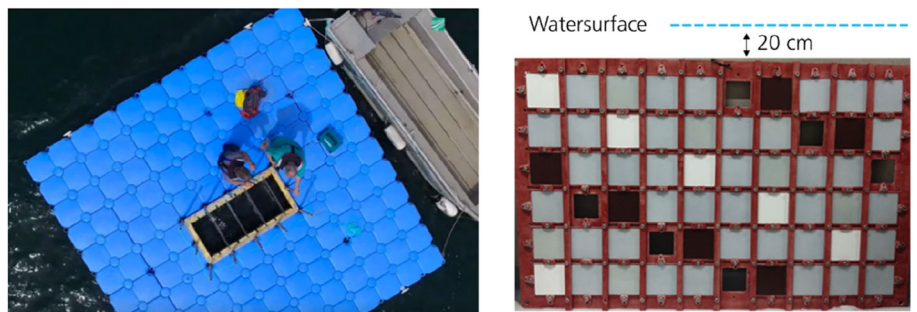


Figure 4. Floating raft for static immersion tests; specimen holder placed in the center of the raft (left), positioning of specimen at the holder (right).

2.6. Calculation of Fouling Portions

Each polymer system is examined by six replicates in the direction of immersion depth (Figure 4 and 5). The surface portion of bare and micro- (MI) and macrofouling (MA) was determined by an image evaluation software which was trained by biologists. Microfouling was characterized by biofilm formation, consisting of slime, microalgae, and fungi. Macrofouling was identified by brown algae, green algae, sponges, tunicates, barnacles, and mussels. The sum of bare, MI, and MA fouling surface portion was 1. The surface portion's average \overline{PS} of bare and micro- and macrofouling x over all replicates m (in direction of the immersion depth) of a polymer system PS was calculated according to

Equation (2) (see also Figure 5). The portion's average of bare, micro- and macrofouling (x) of all polymer systems \overline{PS} was given by PC and was calculated according to Equation (3) (see also Figure 5).

$$\overline{PS}_i = \frac{\sum_{j=1}^m PS_i \cdot j_x}{m} \quad (2)$$

$$PC_x = \frac{\sum_{i=1}^n \overline{PS}_i}{n} \quad (3)$$

with, PS: polymer systems A, B, C, D, E, PR, and NR, PC: polymer classes A, B, C, D, E, PR, and NR, i : number of polymer systems in a polymer class, x : bare B, microfouling MI or

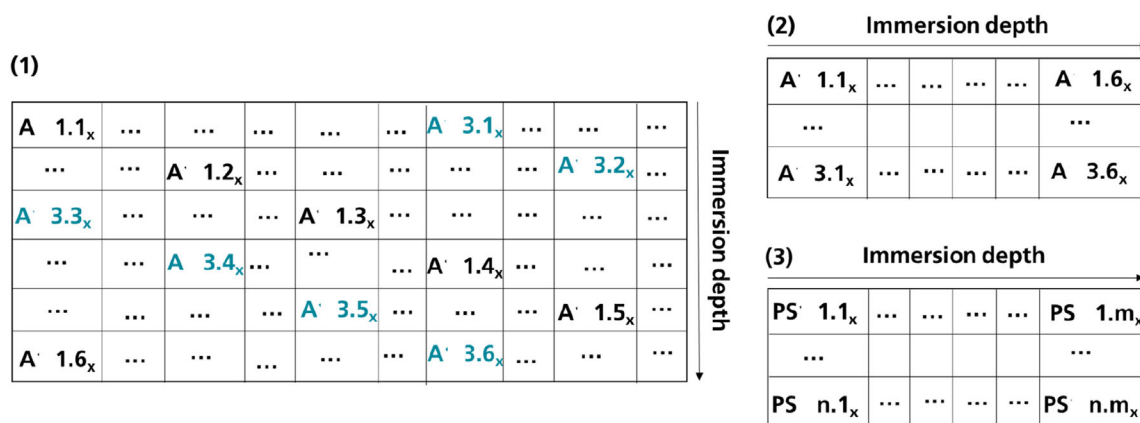


Figure 5. General procedure for the arrangement of samples. 1) Exemplary arrangement on the specimen holder with polymer system A1 and A3 is shown. 2) Rearrangement for graphic documentation of polymer systems in a polymer class, as shown in Figure 10. 3) General description of (2) according to Equation (2), (3), and (5).

macrofouling MA portion, m : number of replicates per polymer system, n : number of polymer systems within the material class.

2.7. Calculation of Fouling-Release Efficiencies

The polymer classes' fouling-release efficiency was based on the bare (B) surface portion and its calculations according to Equation (2) and (3) with

$$\overline{PSi}_B = \frac{\sum_{j=1}^m PSi_{jB}}{m}, \quad PC_B = \frac{\sum_{i=1}^n \overline{PSi}_B}{n} \quad \text{with} \quad (4)$$

$$i = 1, \dots, n; \quad j = 1, \dots, m$$

where PS: polymer systems A, B, C, D, and E, PC: polymer classes A, B, C, D, and E, i : number of polymer systems in a polymer class, B: bare B, m : number of replicates per polymer system, n : number of polymer systems within the material class.

2.8. Calculation of the Polymer System's Performance

Based on the assumption that macrofouling was primarily responsible for a deterioration of hydrodynamic properties and the increase in fuel consumption, no distinction was made between a bare surface and the macrofouling in the presence of macrofouling. Consequently, the performance P or fouling rating FR of a polymer system $P_{\overline{PS},MA}$ or polymer class $P_{PC,MA}$ was related to the macrofouling MA according to ASTM D6990 – 20:2020 given by Equation (5) and (6) as follows

$$P_{\overline{PS},MA} = 1 - \overline{PSi}_{MA} \quad (5)$$

$$P_{PC,MA} = 1 - PC_{MA} \quad (6)$$

with $i = 1, \dots, n$, PS: polymer systems A, B, C, D, and E, PC: polymer classes A, B, C, D, and E, i : number of polymer systems in a polymer class, MA: macrofouling, n : number of polymer systems within the material class.

3. Results

3.1. Effect of Resin-to-Hardener Ratio

Table 5 shows an overview of the adjusted resin-to-hardener ratios and the resulting Young's moduli, Shore 00 hardness, and SFEs, measured after the systems were fully cured (Figure S1, Supporting Information). The interrelations are referred to in the following.

3.1.1. Young's Modulus

The Young's modulus for the commercially available PR Intersleek 1100 SR was measured as 1.5 ± 0.3 MPa ($n = 3$). In sharp contrast, the Young's modulus of the commercially available NR was measured as 1128 ± 114 MPa ($n = 3$). As mentioned (1), the PR's Young's modulus was used as a reference value for the polymer systems considered in the following. Next, attempts were made to affect the crosslinking density and to adjust the Young's modulus of the selected polyurethane- polyurea- and PDMS systems by varying the isocyanate-, hydroxy- and the polydimethylsiloxane - hydride terminated (H-PDMS-H) content, to obtain specimens with a Young's modulus as similar as possible to that of the reference system. According to Table 5, the polyurethane systems A1 to A3 from classes A and B, as well as the polyurea systems C1 to C2 from class C, demonstrate that a reduction in the hardener content n_{eq} lowers the Young's modulus. The Young's modulus of class A range between 0.2 and 2.1 MPa, those of class B between 0.7 and 1.5 MPa, and those of class C between 0.5 and 2.3 MPa. Systems of class A ($R^2 = 0.98$) and class B ($R^2 = 0.91$) exhibit a linear trend between the hardener content n_{eq} and the Young's modulus. The impact of the hardener component n_{eq} with $f1 = \frac{\Delta \text{Young's Modulus} [\%]}{\Delta n_{eq} \text{Hardener} [\%]}$ is calculated for class A with $f1_A = \frac{90.5\%}{22.6\%} = 4$, for class B with $f1_B = \frac{90.5\%}{22.6\%} = 4$, and for class C with $f1_C = \frac{78.3\%}{11.4\%} = 7$. The Young's moduli of the polyurethane systems D1 to D3 were not adjusted via the isocyanate content, but rather through the use of carbinol-terminated siloxane-based binders with different

Table 5. Relationship between hardener (NCO)-, OH-, and PDMS-H (polydimethylsiloxane hydride terminated) amount, Young's modulus, SFE (Wu), and Shore 00 hardness.

Polymer type	Polymer class	Polymer system	$n_{\text{eq,Resin}}, n_{\text{eq,Hardener}}$ [mol%/mol%]	Young's modulus E [MPa]	Young's modulus E , Std. [MPa]	Shore 00	SFE γ [mN m ⁻¹]
Polyurethane	A	A3	50.00/50.00	2.1	0.3	89	22.2
		A2	55.25/44.75	1.1	0.2	77	18.3
		A1	61.73/38.27	0.2	0.1	69	10.3
	B	B3	57.14/42.86	1.5	0.1	87	27.8
		B2	58.82/41.18	0.9	0.1	84	23.4
		B1	60.60/39.40	0.7	0.2	82	19.0
	D	D1 (3.9% OH)	50.00/50.00	2.2	0.2	90	20.9
		D2 (1.6% OH)	50.00/50.00	1.9	0.2	88	25.3
		D3 (0.6% OH)	50.00/50.00	1.0	0.2	82	19.5
Polyurea	C	C2	55.56/44.44	2.3	0.2	n/a	38.5
		C1	60.61/39.39	0.5	0.2	n/a	29.6
			H-PDMS-H content [%]				
PDMS	E	E3	19.07	0.3	0.0	74	23.7
		E2	14.07	0.3	0.0	75	23.0
		E1	9.07	0.4	0.0	77	23.6

equivalent weights and hydroxy contents, respectively. For this purpose, HANSA SFA 92135 (3.9% OH) was used for system D3, HANSA SFA 92075 (1.6% OH) for system D2, and HANSA SFA 92024 (0.6% OH) for system D1. In these systems, a reduction of the Young's modulus is observed with increasing equivalent weight and decreasing hydroxyl content, respectively. The adjusted range of Young's moduli is from 1.0 to 2.2 MPa. The PDMS systems E1 to E3 from class E were prepared via hydrosilylation. An attempt was made to influence the Young's modulus by varying the hydride-terminated component H-PDMS-H. This approach resulted in only minimal changes to the Young's modulus. The adjusted range of the Young's moduli for these systems spans from 0.3 to 0.4 MPa. The Young's moduli across all systems could be set within a range of 0.2 to 2.3 MPa.

3.1.2. Hardness

According to Table 5, the Shore 00 hardness of the systems from classes A and B decreases within each class, like the Young's modulus, with decreasing hardener content n_{eq} . For the systems from class A, Shore 00 hardness values range from 69 to 89 and for systems from class B from 82 to 87. The Shore hardness of the systems from class C could not be determined, as the material surfaces were sticky. Class A ($R^2 = 0.97$) and class B ($R^2 = 0.98$) exhibit a linear relationship between the hardener content n_{eq} and the Shore 00 hardness. The influence of the hardener component n_{eq} , defined as $f_2 = \frac{\Delta \text{Shore 00} [\%]}{\Delta n_{\text{eq,Hardener}} [\%]}$, is calculated for class A to $f_{2A} = \frac{22.8\%}{22.6\%} = 1.0$ and for class B to $f_{2B} = \frac{6\%}{8.1\%} = 0.7$. Within class D, a decrease in Shore 00 hardness with increasing equivalent weight and decreasing hydroxyl content, respectively, can also be observed. The Shore 00 hardness decreases successively from 90 to 82 with decreasing hydroxyl content, although the relationship is not linear. In the systems of class E, unlike the

Young's moduli, a consistently slight reduction in Shore 00 hardness with increasing H-PDMS-H content is observed. The Shore 00 hardness decreases from 77 to 74 as the H-PDMS-H content increases.

3.1.3. SFE

According to Table 5, the SFE of the systems within classes A, B, and C behaves analogously to the Young's modulus and Shore 00 hardness with decreasing hardener content n_{eq} . As the hardener content decreases, the surface energy also decreases. For system A1, strong under-crosslinking results in an exceptionally low surface energy for a polyurethane system, reaching 10.3 mN m⁻¹. The free surface energies for the systems from class A decrease with decreasing hardener content from 22.2 to 10.3 mN m⁻¹, for class B from 27.8 to 19.0 mN m⁻¹, and for class C from 38.5 to 29.6 mN m⁻¹. Class A ($R^2 = 0.98$) and class B ($R^2 = 0.99$) exhibit a linear relationship between the hardener content and the free surface energy. The impact of the hardener component n_{eq} , defined as $f_3 = \frac{\Delta \text{SFE} [\%]}{\Delta n_{\text{eq,Hardener}} [\%]}$ is calculated for class A to $f_{3A} = \frac{53.6\%}{22.6\%} = 2.3$, for class B to $f_{3B} = \frac{16.7\%}{8.1\%} = 2.1$, and for class C to $f_{3C} = \frac{23.2\%}{11.4\%} = 2.0$. The SFEs of the under-crosslinked systems from class D fluctuate and are nonlinear relative to the decrease in hydroxyl content. The surface energies range from 19.5 to 25.3 mN m⁻¹. Similarly, the under-crosslinked systems from class E fluctuate relative to the increase in H-PDMS-H content, with SFEs ranging between 23.0 and 23.7 mN m⁻¹.

3.2. Evaluation of Biofouling during Static Immersion Period

Figure 6 shows the photographic documentation of biofouling on the polymer systems during the entire immersion period and

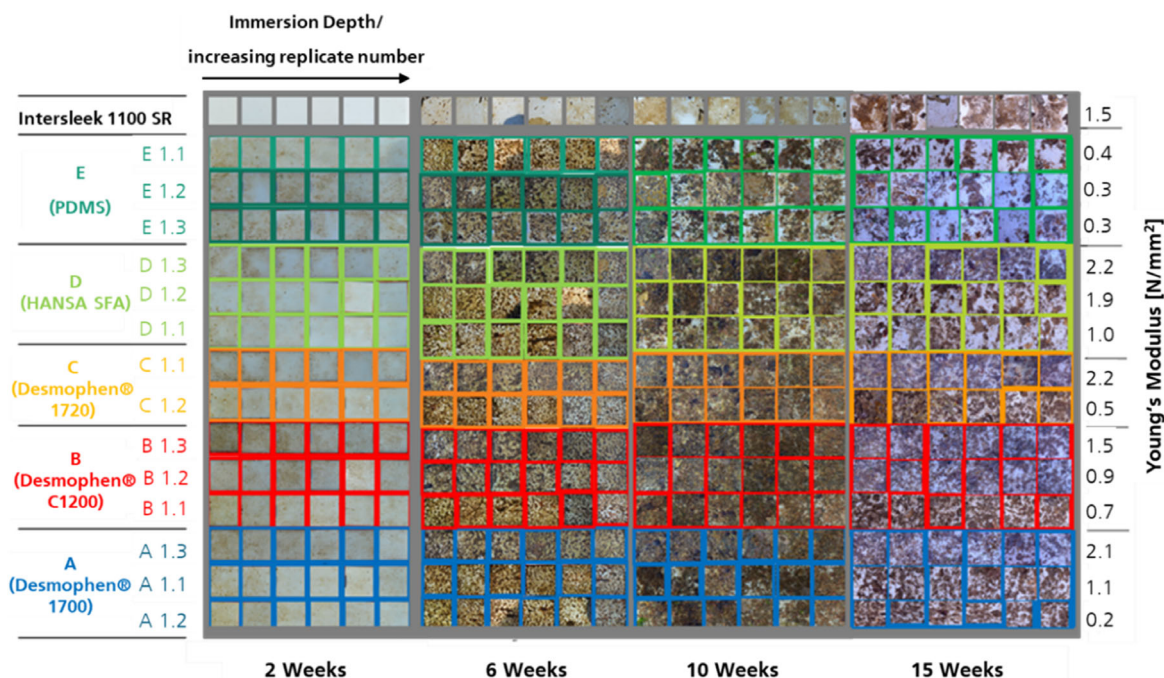


Figure 6. Photographic documentation of immersed polymer systems of classes A (blue), B (red), C (yellow), D (bright green), and E (green) after 2, 6, 10, and 15 weeks from left to right.

provides a qualitative impression of the time-dependent growth of biofouling.

Figure 7 shows the quantitative evaluation of the polymer classes A, B, C, D, E, PR, and NR with their surface portion of bare and micro- and macrofouling, according to Equation (2) and (3). After an immersion period of 2 weeks, the biofouling becomes apparent in the form of microfouling. Macrofouling begins and spreads between 6 and 10 weeks of immersion. Between 10 and 15 weeks of immersion, it seems that a critical force, probably induced either by stronger sea flow or by the own weight of biofouling, leads to detachment of macrofouling, followed by an increase in portion of bare and microfouling.

This can also be reflected in the fouling rate (FR) or performance (P), according to Equation (6), of the polymer class PC. The performance of all material classes decreases over time until the performances converge together with the performance of the PR in week 15; thus, the performance P over all used polymer classes from A to E is $\bar{P}_{A:E,MA} = 0.8 \pm 0.07$ corresponds to that of the PR $P_{PR,MA} = 0.8$ (Figure 11). The reference system seems to require a lower force to initiate the detachment of macrofouling, explaining why the performance seems constant and relatively high at any point during the immersion.

Figure 8 shows the portion of fouling types on the polymer systems of class A to E and its Young's moduli after 2, 6, 10, and 15 weeks. Within a polymer class, there is no correlation between the surface portion of bare and micro- or macrofouling and the Young's modulus, at any time. Since the Young's modulus correlates with the SFE, Shore 00 hardness (Table 5), fouling cannot be correlated to these parameters.

Apart from PR, either the polymer systems from class E or D perform with the highest fouling-release efficiencies (Section 2.7) over the entire immersion period.

Figure 9 shows the relationship between the surface portion and the Young's modulus for all polymer systems, independent from their polymer class. There is also no obvious correlation between the fouling type and Young's modulus at any time. Rather, the fouling behavior of a system with a low Young's modulus seems like a system with a relatively high Young's modulus. For example, Figure 9 at 15 weeks shows the fouling behavior of the polyurethane polymer system A3 and C1 marked by a black frame. Although system A3 has a relatively low Young's modulus and system C1 has a relatively high one, the fouling behavior of both samples seems to be similar. All polymer systems, except for silicone-based systems, exhibit similar amounts of bare surface, microfouling, and macrofouling as the PR. The material appears to be also a key factor, as PDMS-based coatings seem to have the highest fouling-release efficiency with the largest portion of bare area and the smallest portion of micro- and macrofouling (Figure 9, 15 weeks, E2 (PDMS), black frame).

3.3. Evaluation of Biofouling after Static Immersion Period and Increased Hydrodynamic Stress

Figure 10 shows the polymer classes' surface portion of biofouling after the treatment with a high-pressure water jet, applied at 45° and at a distance of a 0.5 m to the samples' surface. The polymer classes' fouling-release efficiency PC_B , according to Equation (3), is given in descending order as follows

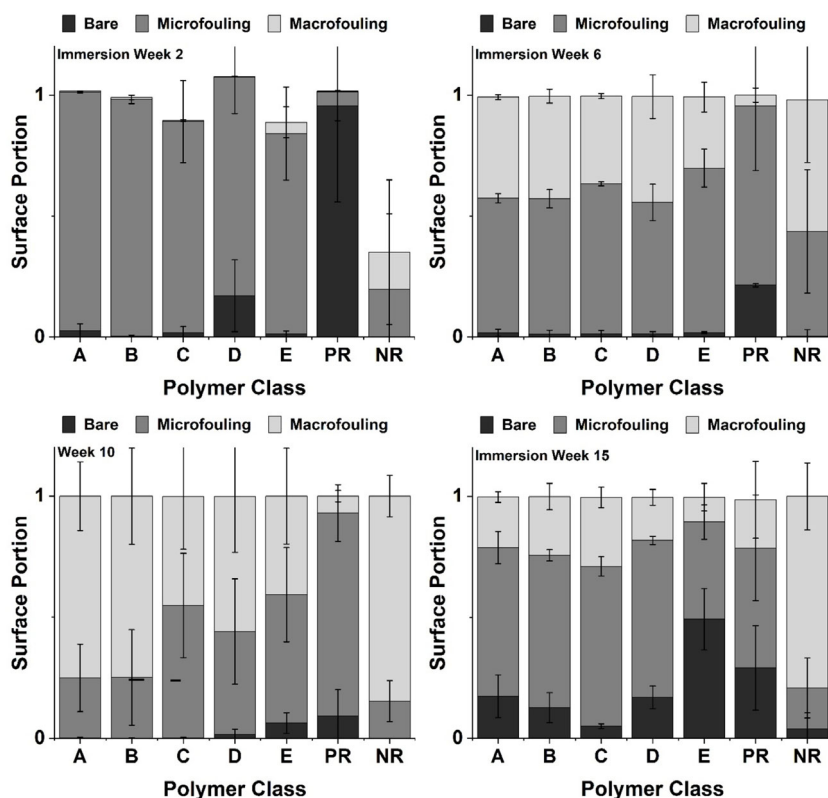


Figure 7. Surface portion of fouling types of all polymer classes, calculated according to Equation (2) and (3), after 2, 6, 10, and 15 weeks of immersion; NR: negative reference, PR: positive reference (Intersleek 1100 SR).

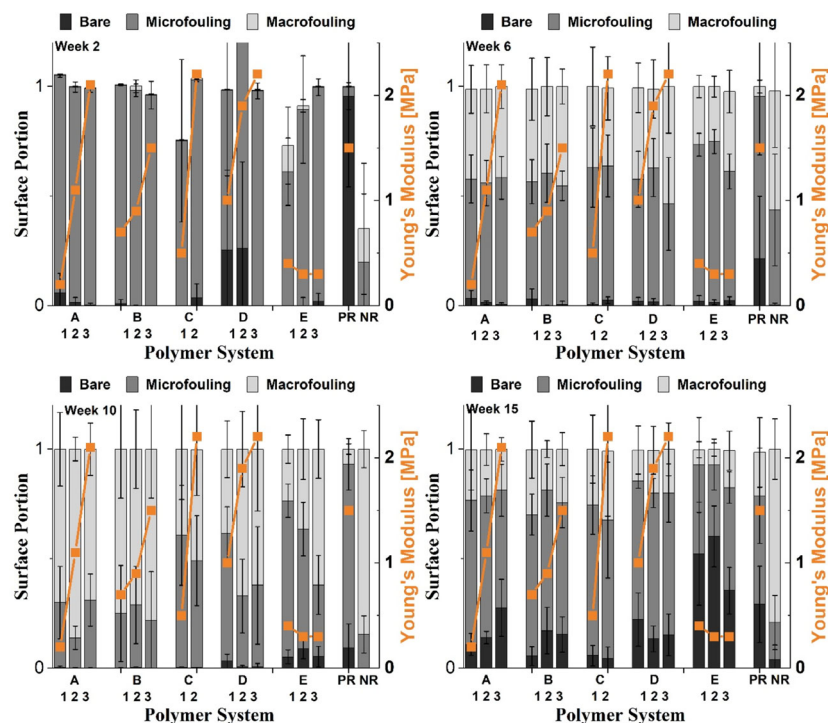


Figure 8. Surface portion of fouling types in dependence on the polymer systems' Young's modulus after 2 and 6 (above) and 10 and 15 (bottom) weeks of immersion. Polymer systems are separated to an increasing Young's modulus within a polymer class. The lines are guides for the eyes.

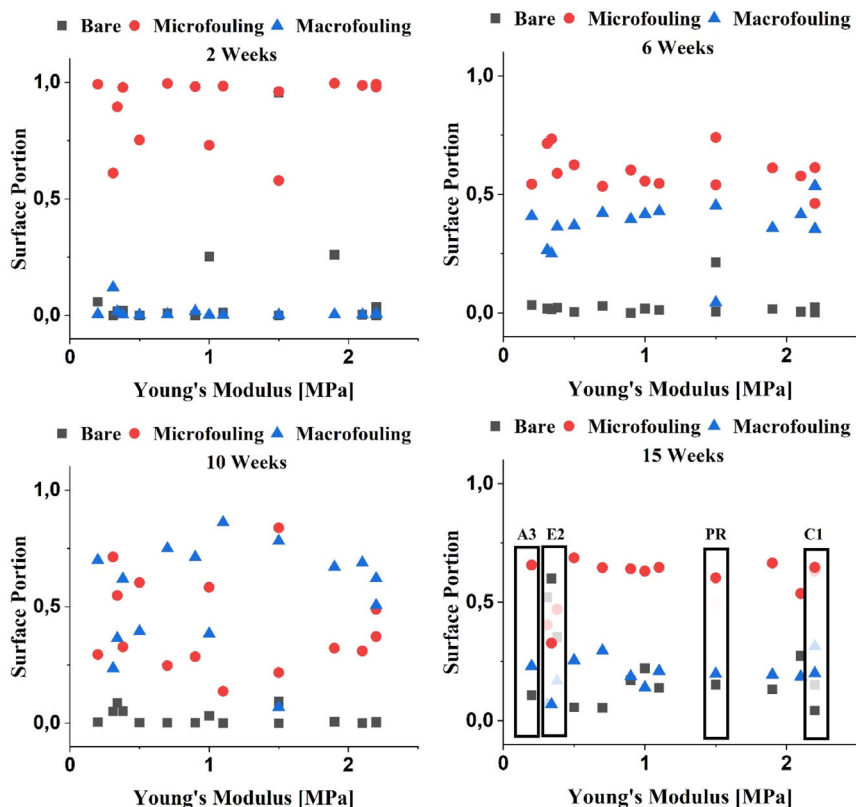


Figure 9. Surface portion of fouling types in dependence on the polymer systems' Young's modulus after 2, 6, 10, and 15 weeks of immersion. Similar fouling behaviors of two polymer systems with low A3 (PUR) and a high C1 (Polyurea) Young's modulus versus fouling behavior of the best performing polymer system E2 (PDMS) with also low Young's modulus, marked by a black frame (week 15). Despite polymer class E (E1 to E3), the fouling type's portions of all polymer systems are close to the ones of the PR (week 15).

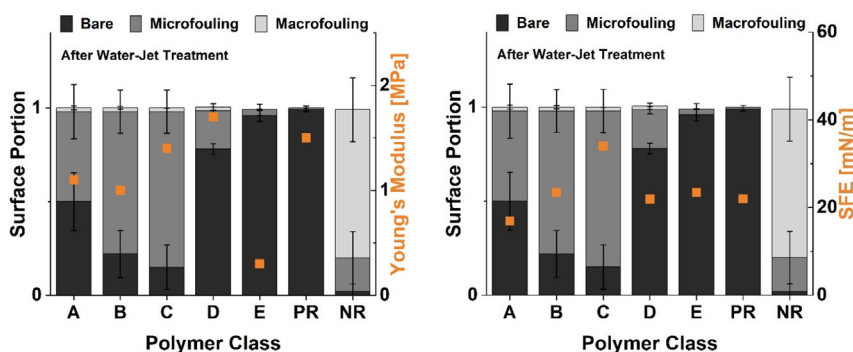


Figure 10. Surface portion of fouling types after high-pressure water jet treatment after week 15 of immersion in dependence on the polymer classes' Young's modulus (left) and SFEs (right).

$$PR_B(0.99) > E_B(0.92) > D_B(0.75) > A_B(0.50) > B_B(0.22) > C_B(0.15) > NR_B(0.02) \quad (7)$$

Apart from the PR's efficiency $PR_B(0.99)$, the efficiency of class $E_B(0.92)$ followed by the efficiency of class D with $D_B(0.75)$ shows the highest fouling-release efficiencies. The difference in the efficiencies between classes E and D is relatively small, but the Young's moduli are at the opposite ends of the Young's modulus' range (Figure 10, left), so that no obvious

relationship between the Young's modulus and the fouling-release efficiency is observed. Apart from the NR, polymer classes A, B, and C with the efficiencies of $A_B(0.50) > B_B(0.22) > C_B(0.15)$ shows the lowest efficiencies of the polymer classes. In this case, the order correlates with its SFE (Figure 10, right), but this relationship does not account for the efficiencies of the remaining polymer classes D and E. The surface energies of polymer classes D and E are similar to those of polymer classes A and B, but the efficiencies are obviously higher (Figure 10, right).

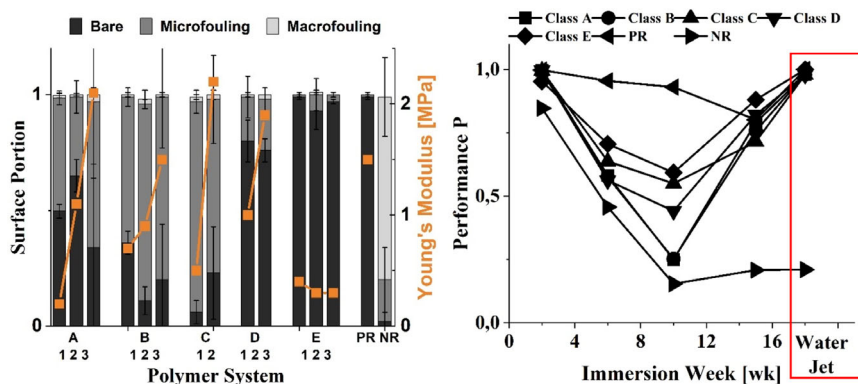


Figure 11. Surface portion of fouling types after 15 weeks of immersion and the high-pressure water jet treatment in dependence on the polymer systems' Young's modulus (left) and performance P of polymer classes during an immersion period of 15 weeks (right) and after using a high-pressure water jet treatment marked by the red frame (right).

Consequently, low Young's modulus and low free surface energy cannot be cited as a general justification for high fouling-release efficiencies.

A deeper look is given by **Figure 11** (left). The plot shows the surface portion of the polymer systems' fouling types in descending order within a polymer class against its Young's moduli. Within a polymer class, there is also no correlation between the system's fouling portions and the systems' Young's moduli.

It appears that the chemical structure of the materials plays a key role in fouling-release efficiency. Thus, the most efficient classes (E and D) are of different material types, polyurethane and PDMS, but both classes contain siloxane units.

Figure 11 (right) shows the performance P of the polymer classes, according to Equation (6) over the entire immersion period of 15 weeks and the performance after the high-pressure water jet treatment. The performance of all polymer classes, excluding the NR, seems to be the same as that of the PR after the high-pressure water jet treatment (red frame), so that P approximately is

$$P_{PR,MA} = P_{A,MA} = P_{B,MA} = P_{C,MA} = P_{D,MA} = P_{E,MA} \quad (8)$$

whereas the performance of the NR remains almost unchanged. In summary, all polymer classes exhibit identical fouling-release performances. Additionally, polymer classes D and E (siloxane-based systems) exhibit the highest, whereas polymer classes C (polyurea) and B (polycarbonate–polyester-based systems) show the lowest fouling-release efficiency.

4. Discussion

4.1. Effect of Varying Resin-to-Hardener Ratio

4.1.1. Young's Modulus

It is well known that reducing the degree of crosslinking in a thermosetting polymer system decreases the resistance of such a system to elastic deformation, thereby decreasing the Young's modulus. Therefore, the Young's moduli of the systems were adjusted by varying the crosslinking density. For the first objective of this work, polymer systems of each polymer class were

chosen whose Young's modulus was as close as possible to that of the Young's modulus of the PR system (1.5 MPa). For the second objective of this work, two additional polymer systems per polymer class with a Young's modulus higher and lower than the first adjusted one were formulated.

As shown in Section 3.1, the Young's moduli of the polyurethane and polyurea systems in classes A, B, and C can be adjusted by varying the resin-to-hardener ratio. Chain flexibility is increased first by a reduction in urethane and urea groups and crosslinking points and second by the associated decrease in both intermolecular and intramolecular hydrogen bonding based on the $-N-H$, $-C=O$, and $-O-R$ groups of the urethane and urea groups. Consequently, under mechanical loading, this leads to an increased strain within the linear-elastic region and thus to a reduction in the Young's modulus. Further reductions of the hardener content were not possible, as the resulting polymer systems were no longer processable.

In contrast to the systems of classes A, B, and C, systems of class E were also synthesized via a polyaddition reaction, but their adjustment in the Young's moduli was not achieved through under-crosslinking, but rather by varying the equivalent weights and the hydroxyl content, respectively, of the carbinol-terminated siloxane binders.

An increase in the equivalent weight, or conversely a decrease in the hydroxyl content of the binder, reduces the amount of urethane and urea groups, thereby lowering the crosslink density and reducing both inter- and intramolecular hydrogen bonding. Consequently, a reduction in the Young's modulus is also observed in these systems.

The polymer systems of class E were synthesized via hydrosilylation, which also constitutes a polyaddition reaction. The intention was to shorten the polymer chain lengths within the network by reducing the amount of H-PDMS-H, thereby creating a more tightly crosslinked network. This, in turn, was intended to limit the material's flexibility and increase its Young's modulus. It was only through this strategy that it became possible to formulate a solid and tensile material.

As shown in the formulation in Table 2, in addition to the relatively strong reduction of the H-PDMS-H component, the amount of the methylhydrosiloxane–dimethylsiloxane copolymer

was also slightly reduced, which may consequently have led to a decrease in crosslinking density. It appears that this effect was too pronounced to result in an increase in Young's modulus. Due to the start of the season, the samples had to be immersed quickly, so that the Young's modulus could only be measured after immersion had begun, making further optimization impossible. The formulation could not be adjusted or further optimized before the systems were immersed in the North Sea, as the Young's modulus of the class E systems could only be measured after immersion. Nevertheless, the material felt noticeably stiffer to the touch.

In general, although it was largely not possible to precisely adjust the Young's modulus to match that of Intersleek 1100 SR, the material parameter could be set and varied within its range. The Young's moduli varied within the scope of manufacturing possibilities, ranging from 0.2 to 2.2 MPa, represent a very narrow range, and vary relatively closely around the Young's modulus of the high-performance FRC Intersleek 1100 SR (PR) of 1.5 MPa, with +0.7 and -1.3 MPa. Despite this relatively small range, an opportunity is given to gain an impression of the sensitivity of the fouling-release properties in relation to the Young's modulus during static immersion and cleaning simulation with a high-pressure water jet. This range does not represent a reference to typical moduli of marine coatings. The standard deviations of the Young's moduli of the polymer systems showed low variations, indicating that preparation was reproducible. For the systems of classes A, B, and C, the impact f_1 of the hardener shows a factor between 4 and 7. Thus, variations in hardener content have the strongest effect on the Young's modulus, relative to their effect on Shore 00 hardness and SFE.

4.1.2. Hardness

A correlation between the stiffness or Young's modulus of a material and its Shore 00 hardness is well known.^[34] The results also indicate that the stiffness and deformation behavior of the materials are reflected in the Shore 00 hardness, resulting in a clear correlation between the Young's modulus and the Shore 00 hardness. Within a class, a reduction in the Young's modulus is accompanied by a corresponding decrease in Shore 00 hardness. Across different classes, this correlation does not hold consistently. For example, while systems in class A exhibit decreasing Shore 00 hardness with decreasing Young's modulus, sample A2 shows a lower Shore 00 hardness (77 Shore 00, 1.1 MPa) than B2 (84 Shore 00, 0.9 MPa) despite having a higher Young's modulus. This discrepancy may be explained by the fact that the impact of the hardener content on the Shore 00 hardness in classes A and B, with $f_2 \leq 1$, which is approximately four times smaller than its effect on the Young's modulus with $f_2 = 4$, making the Shore 00 hardness less sensitive to changes in stiffness and potentially leading to measurement inaccuracies.

4.1.3. SFE

The reduction in SFE observed for the systems in classes A, B, and C as a result of under-crosslinking is remarkable. As previously discussed, the reduction in crosslinking points leads to

increased chain flexibility. In addition, unreacted hydroxyl groups remain in the matrix, and their fraction increases with the degree of under-crosslinking. Due to the enhanced flexibility and the availability of highly polar hydroxyl groups, these polar groups are expected to orient toward the water at the surface, promoting the formation of hydrogen bonds. Consequently, the hydrophilicity and surface energy are anticipated to increase progressively as a result of increasing under-crosslinking. This could not be demonstrated. Possible causes for this could be that the already high-molecular-weight characters of the polymer systems hinder the chains aligning at the water droplet on the surface due to steric hindrance.

Another possible reason is that the proportion of polyurethane groups decreases with the successive under-crosslinking of the systems as mentioned above. This reduces the number of polar hydrogen bonds between the -NH, -C=O, and -O-R groups of the urethane or urea units and the hydroxyl groups of the water droplet. As a result, the polar character of the surface decreases, leading to a reduction in surface energy.

An overlap of both effects may occur, which overall leads to a reduction in SFE. According to the literature, polyurethane, polyurea, and PDMS systems generally exhibit typical SFEs, with the exception of system A1.^[35-37] The polyurethane system A1, which decreases to nearly 10 mN m⁻¹ as a result of successive under-crosslinking, shows a value comparable to strongly nonpolar systems such as PTFE. The impact of the hardener content in classes A, B, and C affects the SFE approximately twice as strongly as it effects Shore 00 hardness.

4.2. Evaluation of Biofouling during Static Immersion Period

Within a single polymer class, no correlation between the Young's modulus and the biorepulsivity can be established at any time during the static immersion period (Figure 7 and 8). But it is evident that the NR, with a significantly higher Young's modulus, consistently exhibits poorer biorepulsivity. It is assumed that the achieved ranges of Young's modulus are too small to measure differences or results in an effect within a polymer class. The sudden increase in fouling-release performance and efficiency (Figure 7-9), characterized by a reduction in macrofouling, an increase in the proportion of uncolonized surface area, and an increase in microfouling—observed in immersion week 15—could be explained by increased hydrodynamic stress, the increased weight of the biofouling, or a combination of both. This suggests that the biorepulsivity of soft materials is activated under the influence of the two mentioned stress factors, because that of the relative hard NR is almost unaffected. Interestingly, all polymer classes are affected by this effect and all polymer classes show the same level of performance compared to the PR. Nevertheless, the fouling-release efficiency of the polymer classes shows differences and is remarkably high for the siloxane-based systems of class E. This is not particularly surprising, as siloxane-based systems,^[13,32] especially PDMS, are considered the standard for FRCs due to its low surface energy and low elastic modulus. But, even though the polyurethane systems from classes A, B, C, and D exhibit surface energies and Young's moduli comparable to those of the PDMS systems in class E, they still demonstrate significantly poorer efficiencies

at all stages of immersion. Therefore, as previously mentioned (Section 3.2), it appears that the chemical nature of the polymer systems, rather than their Young's modulus or SFE, is the key factor for biorepulsivity.

The PDMS backbone consists of siloxane bonds with repeating $[-O-Si-]_n$ units or segment. Due to large bond angles and the reduced rotational energy barrier around the Si-O bond, the chain segments within a polymer chain exhibit high flexibility. As a result, the Si-O-Si backbone can act like a ball joint,^[38] enhancing the flexibility of these chains compared to those with relatively rigid C-C bonds, which are predominant in the systems of classes A, B, C, and D. As a result, nonpolar methyl groups, as is the case in PDMS systems of class E, can arrange themselves around the Si-O-Si backbone and sterically shield it. Consequently, these materials can compensate externally applied forces by material deformation much more sensitively than the materials from classes A, B, C, and D. It is conceivable that the deformation characteristics at the surface have an adverse effect on the adhesion of marine organisms. Additionally, due to the nonpolar character of the methyl groups shielding the Si-O-Si backbone, the PDMS chains can only establish weak intermolecular interactions, such as London dispersion forces, with the adhesives of marine organisms. In contrast, systems from classes A, B, C, and D, based on polyester polyols, polycarbonate polyesters, amine-functional reactants, and carbinol-terminated siloxanes, offer the potential to form significantly stronger polar hydrogen bonds with the adhesives of fouling organisms, due to the presence of the alkoxy, carbonyl, and amino groups. Due to the combination of both the high flexibility of the Si-O-Si backbone, the resulting sensible pronounced material deformation under stress, and the weak physical interactions to the adhesives of fouling organism, fouling organisms on PDMS are sheared off or delaminate from the surface at considerably lower stress, such as those caused by increased seawater flow or the weight of biofouling. This could explain the higher efficiency of PDMS systems compared to the systems of classes A, B, C, and D, despite similar SFEs and Young's moduli. This suggests that the flexibility of chain segments (e.g., $[-Si-O-]_n$) plays a more important role in enhancing the fouling-release character than the Young's modulus and that this cannot necessarily be captured by determining the Young's modulus itself. In any case, the discussion confirms that hydrophobic surfaces, among other factors, promote the fouling-release character. On the other hand, hydrophilic surfaces, e.g., modified by PEG, are attributed with antifouling properties.^[39,40] It can be assumed that the formation of hydrogen bonds to water molecules at the surface leads to hydration and the creation of a "protective layer" against marine organisms. Based on the urethane and urea groups in the systems of classes A, B, C, and D, intermolecular hydrogen bonds with water molecules can also be formed at the interface. Since it has already been demonstrated for systems of classes A, B, and C that the surface energy, and thus the hydrophilic character of the systems, decreases with decreasing crosslink density or decreasing urethane and urea groups (Section 4.1), it is conceivable that the antifouling properties also can be reduced or regulated via the degree of crosslinking. It would therefore be reasonable to expect that systems A1, B1, C1, and D3 exhibit the highest amounts of fouling within their respective classes, as the formation of hydrogen

bonds is expected to be quantitatively the lowest. Across the classes, this would imply, for example, that system C2 should possess stronger antifouling properties than system D3 or any of the other systems. This assumption is not reflected in the experimental observations at any point. One possible explanation could be the binder itself. As previously mentioned, the complete structures of these binders are not fully known, but they contain a plurality of carbonyl, alkoxy, and amino groups that can form hydrogen bonds. Therefore, this unknown number of functional groups could play a much more significant role in determining the antifouling properties, such that variations in crosslinking density and their effect on the formation of hydrogen bonds and the antifouling behavior might be marginal. It is also possible that due to a small overall number of polar groups, or less hydrophilicity, no continuous protective layer is formed—if such a layer forms at all. It is also conceivable that the formation of the layer occurs too slow. Furthermore, it is conceivable that the hydrodynamic load or ocean current has so far been too weak to observe any effects.

4.3. Evaluation of Biofouling after Static Immersion and Increased Hydrodynamic Stress

In contrast to static immersion, significant differences become apparent under a strong hydrodynamic stress by cleaning simulation with a high-pressure water jet. In addition to the PDMS systems from class E, the systems from class D exhibit a significantly increased efficiency E_D due to a higher proportion of free surface area, relative to the polymer systems from classes A, B, and C (Figure 11). Although the systems from class E are also polyurethanes containing a variety of polar urea groups and C-C bonds, which according to Section 4.2 do not contribute to the fouling-release character, they are in fact carbinol-terminated siloxane-based systems and thus also comprise a fraction of PDMS units. The characteristic behavior of siloxanes, or PDMS, described in Section 4.2, now also appears to manifest in the systems from class D under the influence of increased hydrodynamic stress. Since the fraction of PDMS in systems of class D is lower than in the PDMS systems of class E, the efficiency E_B in class E is somewhat less pronounced than the efficiency E_D in system class D, but significantly higher than in the PDMS-free systems from classes A, B, and C. Additionally, in contrast to the static immersion, a linear trend between the free surface energy and the efficiencies PC_B of the systems from classes A, B, and C can be observed after increased hydrodynamic loading (Figure 11). From class C to class A, the surface energy decreases, while the efficiency of the systems increases, as indicated by increasing uncolonized surface and decreasing microfouling. The more hydrophilic the surface becomes, the less pronounced its biorepulsivity is. Contrary to the assumption made in Section 4.2 that an increasing number of urethane groups, or the rising hydrophilic character of the surface, promote the formation of hydrogen bonds with water molecules and could consequently lead to the development of a "protective layer," it appears instead to enhance the interaction with the adhesives of marine organisms. As already mentioned in Section 4.2, it is conceivable that the hydrophilicity of the

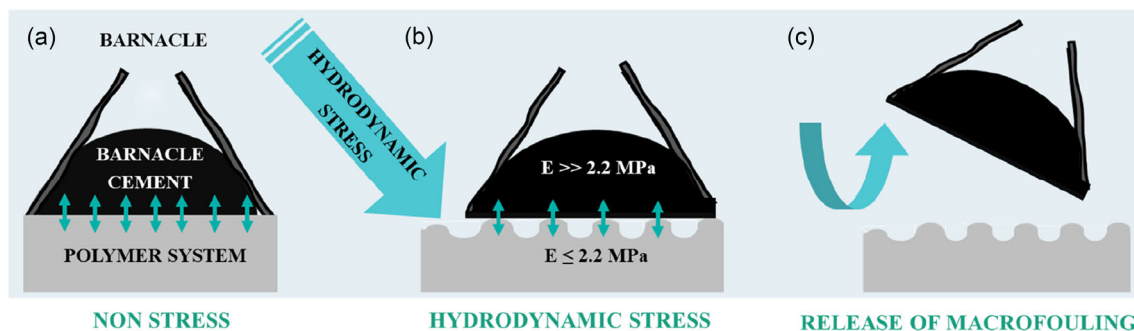


Figure 12. Delamination process of macrofoulers illustrated by the example of a barnacle. a) Nonstressed bonding due to adhesion. b) Hydrodynamic stress—compensation of the induced mechanical load through deformation of the flexible and highly deformable polymer system and the onset of delamination due to insufficient compensation of the induced stress by the rigid barnacle cement. c) Complete overcoming of adhesion and release of macrofouler.

surface is too weakly pronounced for a protective layer to form across the entire area, if it forms at all.

The effect of the low Young's modulus also becomes clearly apparent after the increase in hydrodynamic loading induced by the high-pressure water jet. The assumption that in general the fouling-release efficiency and performance of soft polymer classes correlate with increased hydrodynamic stress was already mentioned in Section 4.2 and is further supported by the cleaning application using a high-pressure water jet. When evaluating the performance of all (soft) polymer classes after treatment, it converges with that of the soft high-performance antifouling coating Intersleek SR1100, resulting in a performance of 1, meaning that macrofouling was completely removed by delamination (Figure 11, right). In contrast to this is the NR, which, unlike the soft polymer classes, has a relatively high Young's modulus and is therefore relatively hard. Delamination of macrofoulers is almost missing. This leads to the following proposal which can be exemplified using a macrofouler such as the barnacle. The proposal is also illustrated in Figure 12. Barnacles adhere irreversibly to an interface by forming a layer of barnacle cement. Depending on the measurement method and barnacle species,^[41] the Young's modulus of barnacle cement can be measured at up to 6.5 GPa, which contrasts sharply with the low Young's moduli of the examined polymer systems of up to 2.2 MPa. The initial situation is defined by a nonstressed state (Figure 12a). Cleaning the surface with a high-pressure water jet induces mechanical stress on the adhesion between the rigid barnacle cement and the soft polymer system (Figure 12b). Barnacle cement is highly rigid and minimally deformable. In contrast, the soft polymer system is highly deformable. The mechanical stress applied to the soft polymer system causes deformation in the adhesive boundary region. The rigid cement is unable to compensate for this deformation, leading to maximum stress on the adhesion at the overlap edges of the layers. These results in adhesive failure, where the shear and peel stresses exerted by the high-pressure water jet led to the delamination of the macrofouler (Figure 12c). Ultimately, the weakness of the adhesion is deliberately exploited to provoke mechanical failure. In contrast, macrofouler delamination does not occur on the NR. Since the NR is relatively hard due to its comparatively high elastic modulus, the substrate undergoes little to

no deformation under induced mechanical stress. As a result, the adhesion strength of the macrofouler is not—or only minimally—challenged, and therefore no delamination occurs.

5. Conclusion

This study demonstrates that the biorepulsivity of the tested polymer coating can be influenced by various material properties. On the one hand, the fouling-release performance increases with a higher portion of flexible and hydrophobic chain segments in the polymer coating, even under low hydrodynamic stress. On the other hand, polar functional groups that tend to form hydrogen bonds can enhance interfacial interactions and increase adhesion between the coating and marine organisms. The Young's modulus, as a mechanical material parameter of a coating, contributes significantly to the delamination process of macrofoulers under increased hydrodynamic stress. Therefore, it can be concluded that the fouling-release properties are governed by the combination of high chain segment flexibility, the type of intramolecular interactions, the nature of intermolecular interactions at the interface between coating and marine organism, the Young's modulus of the coating, and the strength of hydrodynamic stress. Further studies could focus on strategically combining the above-mentioned factors to disrupt the settlement processes of organisms and to further investigate their detachment behavior. With the presented materials, this could be achieved by designing heterogeneous surfaces with domains characterized by gradients in both the Young's modulus and the polarity relative to the surrounding polymer matrix. These domains could be designed with variable dimensions to obtain information on which domain size influences the settlement or detachment processes of the organisms. The detachment behavior of the organisms under varying laminar flow conditions could be observed and evaluated using a flow cell.

Supporting Information

Supporting Information is available from the Wiley Online Library or from the author.

Acknowledgements

This work was carried out within the TransHyDe project Helgoland funded by the German Federal Ministry of Education and Research (BMBF) with the funding code 03HY208C. Financial support is gratefully acknowledged. The authors would like to thank the suppliers for the provided material samples, without which this work would not have been possible. The authors would like to thank their colleagues, Dr. Stübing and Dr. Schreiner, for their input and discussions, as well as for the opportunity to immerse the materials in the North Sea near Helgoland. The authors also extend their gratitude to their colleagues Lars Pospiech, Marius Laur, Andreas Krohn, Tim Heusinger, and Felix Beck for technical support.

Open Access funding enabled and organized by Projekt DEAL.

Conflict of Interest

The authors declare no conflict of interest.

Data Availability Statement

The data that support the findings of this study are available from the corresponding author upon reasonable request.

Keywords

fouling-release coatings, PDMS, polyurea, polyurethane, Young's moduli

Received: June 20, 2025

Revised: September 2, 2025

Published online:

- [1] A. A. Finnie, D. N. Williams, in *Biofouling* (Eds: S. Dürr, J. C. Thomason), Wiley **2009**, pp. 185–206.
- [2] A. G. Nurioglu, A. C. C. Esteves, G. de With, *J. Mater. Chem. B* **2015**, *3*, 6547.
- [3] A. Rosenhahn, T. Ederth, M. E. Pettitt, *Biointerphases* **2008**, *3*, IR1-5.
- [4] M. Lejars, A. Margailan, C. Bressy, *Chem. Rev.* **2012**, *112*, 4347.
- [5] Verordnung (EG) Nr. 782/2003 Des europäischen Parlaments und des Rates vom 14. April 2003 über das Verbot zinnorganischer Verbindungen auf Schiffen, Amtsblatt der Europäischen Union.
- [6] European chemicals agency, <https://echa.europa.eu/de/information-on-chemicals/biocidal-active-substances> (accessed: January 2025).
- [7] International Maritime Organization, [https://www.imo.org/en/OurWork/Environment/Pages/Anti-fouling.aspx#:~:text=AFS%20Convention,The%20International%20Convention%20on%20the%20Control%20of%20Harmful%20Anti%20Dfouling,of%20other%20harmful%20substances%](https://www.imo.org/en/OurWork/Environment/Pages/Anti-fouling.aspx#:~:text=AFS%20Convention,The%20International%20Convention%20on%20the%20Control%20of%20Harmful%20Anti%20Dfouling,of%20other%20harmful%20substances%20) (accessed: March 2025).
- [8] P. Marzullo, M. Gruttadauria, F. D'Anna, *Biomolecules* **2024**, *14*, 957.
- [9] S. Wang, B. Qiu, J. Shi, M. Wang, *J. Coat. Technol. Res.* **2024**, *21*, 87.
- [10] S. Kliewer, S. G. Wicha, A. Bröker, T. Naundorf, T. Catmadim, E. K. Oellingrath, M. Rohnke, W. R. Streit, C. Vollstedt, H. Kipphardt, W. Maison, *Colloids Surf., B* **2020**, *186*, 110679.
- [11] H. S. Sundaram, Y. Cho, M. D. Dimitriou, C. J. Weinman, J. A. Finlay, G. Cone, M. E. Callow, J. A. Callow, E. J. Kramer, C. K. Ober, *Biofouling* **2011**, *27*, 589.
- [12] A. Rahimi, S. J. Stafslin, L. Vanderwal, J. Bahr, M. Safaripour, J. A. Finlay, A. S. Clare, D. C. Webster, *Langmuir* **2021**, *37*, 2728.
- [13] E. Guazzelli, F. Perondi, F. Criscitiello, C. Pretti, M. Oliva, V. Casu, F. Maniero, L. Gazzera, G. Galli, E. Martinelli, *J. Mater. Chem. B* **2020**, *8*, 9764.
- [14] S. Bauer, M. P. Arpa-Sancet, J. A. Finlay, M. E. Callow, J. A. Callow, A. Rosenhahn, *Langmuir* **2013**, *29*, 4039.
- [15] D. Akuzov, T. Vladkova, G. Zamfirova, V. Gaydarov, M. V. Nascimento, N. Szeglat, I. Grunwald, *Prog. Org. Coat.* **2017**, *103*, 126.
- [16] J. F. Karthäuser, J. Koc, E. Schönemann, R. Wanka, N. Aldred, A. S. Clare, A. Rosenhahn, A. Laschewsky, *Adv. Mater. Interfaces* **2022**, *9*, 2200677.
- [17] E. Schönemann, J. Koc, N. Aldred, A. S. Clare, A. Laschewsky, A. Rosenhahn, E. Wischerhoff, *Macromol. Rapid Commun.* **2020**, *41*, e1900447.
- [18] J. Koc, E. Schönemann, A. Amuthalingam, J. Clarke, J. A. Finlay, A. S. Clare, A. Laschewsky, A. Rosenhahn, *Langmuir* **2019**, *35*, 1552.
- [19] J. F. Karthäuser, R. Kopecz, E. Schönemann, A. Martínez Guajardo, A. Laschewsky, A. Rosenhahn, *Adv. Mater. Interfaces* **2024**, *11*, 2300873.
- [20] L. Schardt, A. Martínez Guajardo, J. Koc, J. L. Clarke, J. A. Finlay, A. S. Clare, H. Gardner, G. W. Swain, K. Hunsucker, A. Laschewsky, A. Rosenhahn, *Macromol. Rapid Commun.* **2022**, *43*, 2100589.
- [21] E. Schönemann, J. Koc, J. F. Karthäuser, O. Özcan, D. Schanzenbach, L. Schardt, A. Rosenhahn, A. Laschewsky, *Biomacromolecules* **2021**, *22*, 1494.
- [22] S. K. Rath, J. G. Chavan, T. K. Ghorpade, T. Umasankar Patro, M. Patri, *J. Coat. Technol. Res.* **2018**, *15*, 185.
- [23] Y. Zhang, Y. Qi, Z. Zhang, *Prog. Org. Coat.* **2016**, *97*, 115.
- [24] H. O. G. Benschop, A. J. Guerin, A. Brinkmann, M. L. Dale, A. A. Finnie, W.-P. Breugem, A. S. Clare, D. Stübing, C. Price, K. J. Reynolds, *Biofouling* **2018**, *34*, 532.
- [25] R. F. Brady, I. L. Singer, *Biofouling* **2000**, *15*, 73.
- [26] R. F. Brady, *Prog. Org. Coat.* **2001**, *43*, 188.
- [27] J. Y. Chung, M. K. Chaudhury, *J. Adhes.* **2005**, *81*, 1119.
- [28] R. F. Brady, *Prog. Org. Coat.* **1999**, *35*, 31.
- [29] R. A. D. Baier, R. E. Baier, V. A. DePalma, in *Management of Arterial Occlusive Disease* (Ed: W. A. Dale), Year Book Medical Publishers, Inc., Chicago **1971**, pp. 147–163.
- [30] R. E. Baier, *J. Mater. Sci.: Mater. Med.* **2006**, *17*, 1057.
- [31] R. Xie, X. Ai, Q. Xie, C. Ma, G. Zhang, *Prog. Org. Coat.* **2023**, *175*, 107350.
- [32] M. K. Chaudhury, J. A. Finlay, J. Y. Chung, M. E. Callow, J. A. Callow, *Biofouling* **2005**, *21*, 41.
- [33] S. Jalali, M. Tafazzoli-Shadpour, N. Haghighipour, R. Omidvar, F. Safshekan, *Cell Commun. Adhes.* **2015**, *22*, 79.
- [34] A. N. Gent, *Rubber Chem. Technol.* **1958**, *31*, 896.
- [35] relyon plasma, <https://www.relyon-plasma.com/kunststoffe/> (accessed: May 2025).
- [36] tantec Deutschland, <https://www.tantec-deutschland.de/glossar/oberflaechenspannung-von-kunststoffen> (accessed: May 2025).
- [37] innotape, <https://www.innotape.de/blog/oberflaechenenergie> (accessed: May 2025).
- [38] M. Grübel, *Analyse und Funktionalisierung Siloxanbasierter Thermoplastischer Elastomer*, Technische Universität München **2016**.
- [39] C. Wei, Y. Zhang, Z. Tang, C. Zhang, J. Wu, B. Wu, *Polymers* **2024**, *16*, 1570.
- [40] Z. Zhou, D. R. Calabrese, W. Taylor, J. A. Finlay, M. E. Callow, J. A. Callow, D. Fischer, E. J. Kramer, C. K. Ober, *Biofouling* **2014**, *30*, 589.
- [41] V. Zheden, W. Klepal, S. N. Gorb, A. Kovalev, *Interface Focus* **2015**, *5*, 20140049.